Article

Advanced Materials: Nature of Strongly Correlated Quantum Spin Liquid in $Sr_3CuNb_2O_9$

Vasily R. Shaginyan [1,2,*], Alfred Z. Msezane [2], Stanislav A. Artamonov [1] and Yalia S. Leevik [3]

[1] Petersburg Nuclear Physics Institute, NRC Kurchatov Institute, Gatchina 188300, Russia; artamonov_sa@pnpi.nrcki.spb (S.A.A.)

[2] Department of Physics, Clark Atlanta University, Atlanta, GA 30314, USA; AMsezane@cau.edu (A.Z.M.)

[3] Higher School of Economics, National Research University, Moscow 194100, Russia; ysl1968@mail.ru (Y.S.L.)

* Corresponding author. E-mail: vrshag@thd.pnpi.spb.ru (V.R.S.)

ABSTRACT: Quantum spin liquids of frustrated magnets are among the most attractive and basic systems in physics. Frustrated magnets exhibit exceptional properties as insulators and metals, making them advanced materials that represent materials for future technologies. Therefore, a reliable theory describing these materials is of great importance. The fermion condensation theory provides an analytical description of various frustrated quantum spin liquids capable of describing the thermodynamic and transport properties of magnets based on the idea of spinons, represented by chargeless fermions filling the Fermi sphere up to the Fermi momentum p_F. We show that the low temperature thermodynamic of $Sr_3CuNb_2O_9$ in magnetic fields is defined by strongly correlated quantum spin liquid. Our calculations of its thermodynamic properties agree well with recent experimental facts and allow us to reveal their scaling behavior, which is very similar to that observed both in heavy-fermion metals and in frustrated magnets or insulators. We demonstrate for the first time that $Sr_3CuNb_2O_9$ belongs to the family of strongly correlated Fermi systems that form a new state of matter.

Keywords: Quantum phase transitions; Flat bands; Quantum spin liquid; Thermodynamic properties; Scaling behavior; Universal properties; Heavy fermion metals

1. Introduction

Explaining the universal behavior of thermodynamic and transport properties of a wide variety of strongly correlated Fermi systems remains one of the major challenges in condensed matter physics. Strongly correlated Fermi systems are represented by heavy fermion (HF) metals, high-T_c superconductors, frustrated magnets/insulators with quantum spin liquid, quasicrystals, *etc.* To explain the universal behavior, it is reasonable to assume that the universal behavior is related to a quantum phase transition that shapes the behavior of a strongly correlated Fermi system located near the transition, see e.g., and Refs therein [1–3]. It has been shown that in a wide variety of substances and under a broad variety of external conditions, the topological fermion condensation phase transition (FCQPT) occurs [1,4,5]. This phase transition defines the macroscopic properties and behavior of strongly correlated substances, the number of which is growing exponentially, see e.g., [6]. All these substances can reasonably be considered as a new state of matter, because their behavior near the phase transition acquires important similarities that make them universal. The idea of such a phase transition creating flat bands has been in the works for a long time, first as a curious mathematical possibility [4,7] and now as a rapidly developing, a dynamic area with countless applications, see e.g., [1,2,5,8–15]. Therefore, it is very important to identify new materials that have the universal behavior of their properties.

Recently $Sr_3CuNb_2O_9$ has been exposed as a disorder-induced random three-dimensions (3D) spin singlet state and a quantum spin liquid (QSL) state [16]. Such a disorder-induced random spin singlet state leads to a frustration generating a huge accidental degeneracy of different spin configurations that is known as QSL state. Experimental data revealed no evidence of long-range magnetic order or spin freezing up to 466 mK [16]. Since QSL supports all possible spin partitions into valence bonds, its ground state is highly degenerate. This is another consequence of the initial geometric frustration. To understand the significance of exotic excitations, recall that typically in condensed matter physics, excitations (quasiparticles) are associated with, for example, electrons, *i.e.*, fermions with spin 1/2 and charge

$\pm e$, and phonons, or magnons, *i.e.*, bosons with integer spin ($S = 1$ for magnons and $S = 0$ for phonons). In QSL, the most familiar exotic excitations are spinons, which in 3D can be thought of as "empty space", *i.e.*, a spin that is not paired in a valence bond. Such spinons form a Fermi sphere with Fermi momentum p_F and can move by rearranging nearby valence bonds with low energy costs [9]. They carry spin $S = 1/2$ and have no electric charge. Note that, unlike metals, spinons cannot support a charge current, but they can, for example, transport heat, as do electrons of metals. It can be suggested that the presence of these exotic excitations requires a special theoretical description. Our goal is to clarify the nature of QSL in terms of the phenomenon of fermion condensation (FC), which generates flat bands, they were theoretically predicted [7] and described in detail in [1,4,5]. The necessary ingredients for the realization of FC in quantum frustrated magnets are flat bands, *i.e.*, the dispersionless parts of QSL that form the quasiparticle spectra. Our aim is to clarify the nature of QSL in terms of the phenomenon of FC, which forms flat bands. It turns out that the best candidates for realizing such flat bands are strongly correlated Fermi systems, such as heavy-fermion metals (HF), high-T_c superconductors and quantum frustrated magnets, see e.g., [6].

The topological FCQPT [1,5] forming flat bands can be considered as quantum critical point (QCP) of the quantum spin liquid $Sr_3CuNb_2O_9$. Thus, we can safely assume that the deconfined Fermi quantum spin liquid with essentially gapless excitations formed by neutral fermions, *i.e.*, spinons, is realized in quantum frustrated magnets like $Sr_3CuNb_2O_9$ and is located very close to QCP. Thus, $Sr_3CuNb_2O_9$ appears to be in its QCP without tuning this substance to its QCP using a controlling parameter such as magnetic field B, pressure or chemical composition, and its QSL can be viewed as the strongly correlated quantum spin liquid. Thus, SCQSL consists of chargeless heavy spinons with $S = 1/2$ and effective mass M^*, occupying the corresponding Fermi sphere with Fermi momentum p_F. This befalls because one frustrated valence spin is taken to fill an approximately flat spinon band. This physics is very similar to the physics of HF metals, whose valence electrons form approximately flat conduction bands. Since the negative charges $-e$ cannot form any band filled with wandering bosons (*i.e.*, spinless electrons) due to the large charge gap in the geometrically frustrated insulating magnet, this leads to spin-charge separation. Thus, frustrated magnetic insulators such as $Sr_3CuNb_2O_9$, HF metals and other strongly correlated Fermi systems exhibit universal scaling behavior, forming the new state of matter [5].

In our paper, we focus on $Sr_3CuNb_2O_9$, which is a new frustrated or highly disordered magnet, represented as a disorder-induced random three-dimensional (3D) spin singlet state with its quantum spin liquid (QSL) state [16]. We show that QSL is represented by strongly correlated quantum spin liquid (SCQSL) [5,17]. We describe QSL and its QCP in $Sr_3CuNb_2O_9$, and explain its phase diagram and low temperature thermodynamics in magnetic fields B. We calculate the magnetization M, the field dependence of dM/dT and magnetic specific heat C_{mag}/T as functions of temperature T versus magnetic field B. Our analysis agrees well with experimental facts and reveals their scaling behavior, which is very similar to that observed in both HF metals and frustrated QSL magnets. We demonstrate for the first time that $Sr_3CuNb_2O_9$ belongs to the family of strongly correlated Fermi systems that form the new state of matter.

The paper is organized as follows. In Section 2 we present brief exposition of the FC theory. In Section 3 a schematic $T - B$ phase diagram and the scaling behavior of QSL in the geometrically frustrated magnets $Sr_3CuNb_2O_9$ are considered. We demonstrate that the QSL $Sr_3CuNb_2O_9$ exposes the behavior of heavy-fermion metals, with one exception: it does not support electric current. Section 4 summarizes the main results of the paper and describes the prospects for searching for QSLs in frustrated magnets.

2. Low Temperature Thermodynamic

To analyze the thermodynamic properties and their scaling behavior at low temperatures, we the model of the homogeneous HF liquid [1,5]. This model avoids complications associated with the crystalline anisotropy of solids. We assume that the quantum spin liquid $Sr_3CuNb_2O_9$ consists of fermions. These fermions with zero charge and spin $\sigma = 1/2$ occupy the corresponding Fermi sphere with the Fermi momentum p_F. The quasi-cubic 3D structure $Sr_3CuNb_2O_9$ generates a 3D frustrated lattice, which in turn generates a frustrated QSL [16]. As a result, we safely assume that the single-particle QSL spectrum is characterized by a flat band associated with the topological FCQPT. As a result, strongly correlated Fermi systems located near the topological FCQPT exhibit universal scaling behavior.

In this case, the ground state energy $E(n)$ is given by the exact Landau functional, which depends on the quasiparticle distribution function $n_\sigma(\mathbf{p})$, where $\mathbf{p}$ is the momentum [18]. Near the topological FCQPT, the effective mass M^* is

determined by the exact Landau equation [1,18,19]

$$\frac{1}{M^*(T,B)} = \frac{1}{M^*} + \frac{1}{p_F^2} \sum_{\sigma_1} \int \frac{\mathbf{p_F p_1}}{p_F}$$

$$\times \quad F_{\sigma,\sigma_1}(\mathbf{p_F}, \mathbf{p_1}) \frac{\partial \delta n_{\sigma_1}(\mathbf{p_1}, T, B)}{\partial \mathbf{p_1}} \frac{d\mathbf{p_1}}{(2\pi)^3}. \tag{1}$$

Here we rewrite the quasiparticle distribution function as $n_\sigma(\mathbf{p}, T, B) \equiv n_\sigma(\mathbf{p}, T = 0, B = 0) + \delta n_\sigma(\mathbf{p}, T, B)$. The Landau amplitude F is completely fixed by the fact that the system must be in FCQPT [1,20,21]. The only role of the Landau amplitude is to bring the system to the point FCQPT, where the Fermi surface changes its topology so that the effective mass becomes strongly dependent on the temperature T and magnetic field B [1,20]. At the point FCQPT the term $1/M^*$ disappears and Equation (1) becomes homogeneous. As a result, it is solved analytically [1,20]. At $B = 0$, the effective mass depends strongly on T, exhibiting NFL behavior [1,20]

$$M^*(T) \simeq a_T T^{-2/3}. \tag{2}$$

At finite T, applying a magnetic field B moves the system into the LFL region with M^* depending on B

$$M^*(B) \simeq a_B B^{-2/3}. \tag{3}$$

For finite B and T near the topological FCQPT, solutions of Equation (1) $M^*(B, T)$ can be easily approximated by a simple universal interpolation function. This interpolation takes place between the regions LFL ($M^*(T) \propto const$) and NFL ($M^*(T) \propto T^{-2/3}$) [1,20]. It is appropriate to introduce the normalized effective mass M_N^* and the normalized temperature $_N$, dividing the effective mass M^* by its maximum values, M_M^*, and the temperature T by $T_{\max}$, at which the maximum is reached, as shown in the inset of the phase diagram Figure 1.
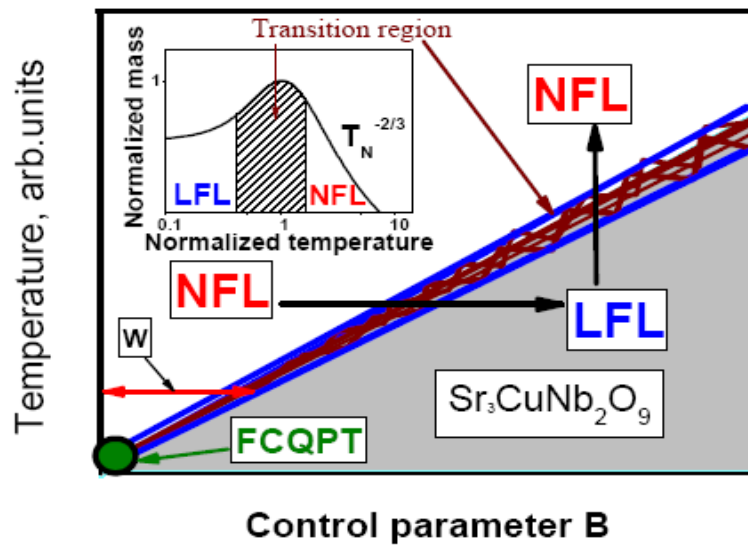

Figure 1. The schematic $T - B$ phase diagram of $Sr_3CuNb_2O_9$. The vertical and horizontal arrows show the LFL-NFL and NFL-LFL crossovers for fixed B and T, respectively. The inset shows a plot of the normalized effective mass M_N^* versus normalized temperature T_N. The crossover region where M_N^* reaches its maximum $M_N^* = 1$ at $T_N = T/T_{\max} = 1$ is shown by the arrows and the shaded area in both the main panel and the inset. As the temperature T and magnetic field B decrease, the length of the red arrow, designated W, tends to zero and the system comes to the topological FCQPT.

The normalized effective mass $M_N^* = M^*/M_M^*$ as a function of the normalized temperature $y = T_N = T/T_{\max}$ is determined by the interpolation function [1,20]

$$M_N^*(y) \approx c_0 \frac{1 + c_1 y^2}{1 + c_2 y^{8/3}}. \tag{4}$$

Here $c_0 = (1 + c_2)/(1 + c_1)$, c_1 and c_2 are adjustable parameters approximating the Landau amplitude. The magnetic field B enters into Equation (1) only in combination $\mu_0 B/k_B T$, making $k_B T_{\max} \simeq \mu_0 B$, where k_B is the Boltzmann

constant and μ_0 is the Bohr magneton [1,20]. Thus, when magnetic fields are applied, the variable y becomes

$$y = T/T_{\max} \simeq k_B T / \mu_0 B. \tag{5}$$

The variables T and B enter Equation (5) symmetrically; therefore, Equation (4) is valid for $y = \mu_0 B / k_B T$. In what follows, we use Equation (4) to explain our calculations based on Equation (1). From Equations (3), (4) and (5), it follows directly from this that

$$T^{2/3} \chi(k_B T / \mu_0 B) \propto y^{2/3} M_N^*(y). \tag{6}$$

Thus, $T^{2/3} \chi(k_B T / \mu_0 B)$ depends only on the variable y and determines the scaling behavior. The T dependence of $\chi(T)$ is defined by Equation (2)

$$\chi(k_B T / \mu_0 B) \propto T^{-2/3}. \tag{7}$$

As we will see below, this result is in good agreement with experimental facts [16].

Equation (4) allows one to calculate the universal thermodynamic properties of strongly correlated Fermi systems. Indeed, these properties become universal and independent of the microscopic properties of the system under consideration after the normalization procedure [1,5]. For example, the normalized susceptibility $\chi_N = \chi/\chi_{\max} = M_N^*$. Since $C/T \propto M^*$, then the normalized $(C/T)_N = \chi_N = M_N^*$. Note that our M_N^* calculations based on Equation (1) do not include any free fitting parameters.

Now consider the magnetization: since the magnetization

$$M(B,T) = \int \chi(B,T) dB, \tag{8}$$

where $\chi(B,T) \propto B^{-2/3}$, see Equation (3). From Equations (4), (6) and (8) we find that

$$M(B,T) = \int \chi(B,T) dB \propto T^{1/3} \int M_N(y) y^{2/3} dy. \tag{9}$$

Thus, it follows from Equation (9) that $M(B,T) T^{-1/3}$ depends on the only variable $y \propto \mu_0 B / k_B T$. These observations are in good agreement with the scaling behavior of $MT^{-0.35}$ and $\chi \propto T^{-0.63}$ experimentally established in Ref. [16]. It also directly follows from Equation (9) that

$$B^{2/3} \frac{M(B,T)}{dT} = F(T/B), \tag{10}$$

where $F(T/B)$ is a function calculated using the Equation (9), while $2/3 \simeq 0.63$ is in good agreement with experimental measurements [16].

3. Phase Diagram and Scaling Behavior of $Sr_3CuNb_2O_9$

Let us proceed to construct the schematic phase diagram of the frustrated magnet $Sr_3CuNb_2O_9$, the behavior of which is determined by SCQSL. The phase diagram is shown in Figure 1. At $T = 0$ and $B = 0$, SCQSL is in FCQPT without adjustment. Both temperature T and magnetic field B, which are the control parameters, shift SCQSL out of the topological FCQPT and move it from the NFL to LFL regions, as shown by the vertical and horizontal arrows. At fixed temperatures, increasing B moves the system along the horizontal arrow from the NFL region to the LFL region. In contrast, at a fixed B and increasing temperature, SCQSL moves along the vertical arrow from the LFL region to the NFL region. The inset to Figure 1 demonstrates the universal behavior of the normalized effective mass M_N^* as a function of the normalized temperature T_N, following from Equation (4). From Figure 1 it is evident that the temperature region $T_N \sim 1$ is a transition region between the LFL behavior with a nearly constant effective mass M^* and the NFL behavior with the dependence $M^*(T) \propto T^{-2/3}$. From Equations (4) and (5) and Figure 1 it is obvious that the width of the transition region behaves as $T_w \propto T \propto B$.

Now let us move on to considering the thermodynamic function. Figure 2, panel (a), presents the scaled magnetization $M(\mu_0 B / k_B T)$ measured on $Sr_3CuNb_2O_9$ [16], and Figure 2, panel (b), shows the scaled magnetization collected on $ZnCu_3(OH)_6Cl_2$ [22]. It is clearly seen that the data collected on both $Sr_3CuNb_2O_9$ and $ZnCu_3(OH)_6Cl_2$ collapse into the same curve, obeying the scaling behavior. It is seen from Figure 2 that the different frustrated $Sr_3CuNb_2O_9$ and $ZnCu_3(OH)_6Cl_2$ expose the same scaled behavior of $M(\mu_0 B / k_B T)$, given by Equation (9), and are in good agreement with the experimental facts.
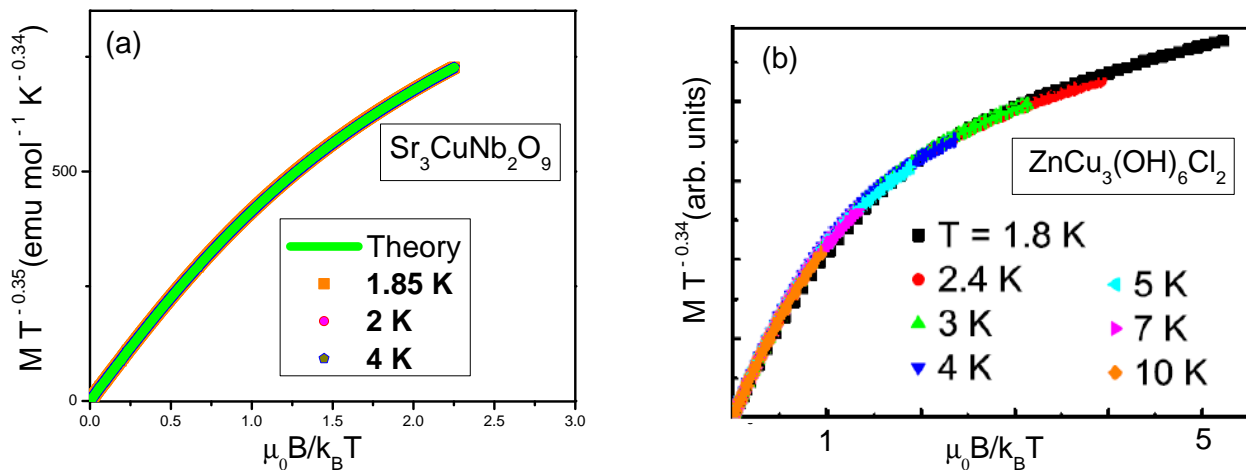
Figure 2. Scaling behavior of the magnetization $M(B, T)$ as a function of magnetic field B at different temperatures T. Panel (**a**): $M \propto T^{-0.35}$. Scaled magnetization $MT^{-0.35}(y)$ collected on measurements on $Sr_3CuNb_2O_9$ with $y = \mu_0 B/k_B T$ [16] . Panel (**b**): Scaled magnetization $MT^{-0.34}(y)$ collected on $ZnCu_3(OH)_6Cl_2$ [22]. In both cases, measurements are carried out at different temperatures indicated in the corresponding legends.

Figure 3a displays the scaled plot of the magnetic susceptibility $\chi T^{0.66}$ measured on the insulator $ZnCu_3(OH)_6Cl_2$ [22]. Since at $\mu_0 B/k_B T \leq 1$ the magnetic susceptibility χ exhibits the NFL behavior, $\chi \propto T^{-0.66}$, see Equation (2), therefore, $\chi T^{0.66}$ is approximately constant, as seen from Figure 3a. It is seen from Figure 3b that in zero magnetic field $B = 0$ the same behavior is demonstrated by $Sr_3CuNb_2O_9$ [16], $\chi \propto T^{-0.63}$, that confirms that the both compounds exhibit the NFL behavior.
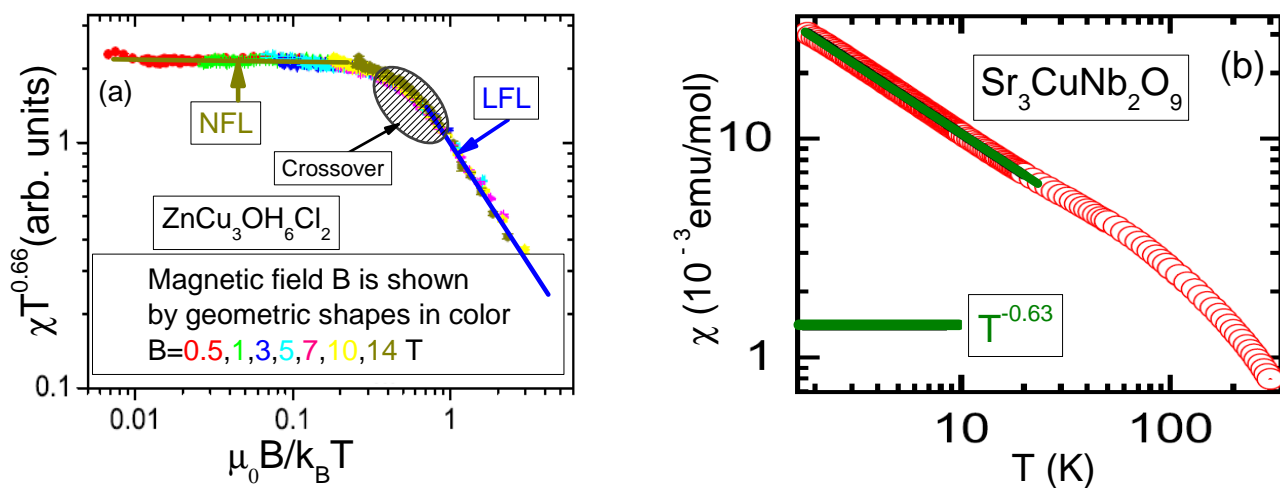

Figure 3. Magnetic susceptibility χ. Panel (**a**): Scaled plot of the magnetic susceptibility $\chi T^{0.66}$ as a function of $\mu_0 BH/k_B T$ collected on $ZnCu_3(OH)_6Cl_2$ [22] and measured under the application of magnetic field B shown in the legend. The NFL behavior at $\mu_0 BH/k_B T \leq 1$ is shown by the straight line. Consistent with the phase diagram displayed in Figure 1, at growing the magnetic field ($\mu_0 BH/k_B T \sim 1$) NFL behavior is first transformed into crossover behavior and then degenerates into LFL behavior under the influence of magnetic field at $\mu_0 BH/k_B T \geq 1$. The crossover is shown as a shaded area, and the NFL behavior is outlined by the straight line. Panel (**b**) shows the power-law behavior of the susceptibility χ measured on $Sr_3CuNb_2O_9$ at nonzero applied field of $B = 1$ T [16]. The straight line demonstrates that at $2 < T < 20$ K the susceptibility displays the NFL behavior $\chi \propto T^{-0.63}$, see Equation (2). Thus, the both $ZnCu_3(OH)_6Cl_2$ and $Sr_3CuNb_2O_9$ display the same NFL behavior.

Consider the magnetization difference dM/dT. Taking into account that $dM/dT = dS(B,T)/dB$, see e.g., [23]. Now let us consider the evolution of the derivative of the magnetic entropy $dS(B,T)/dB$ as a function of the magnetic field B. This derivative is important because allows to analyze the scaling behavior of the derivative of the effective mass $dM^*(B,T)/dT = dS(B,T)/dB$, given by Equation (4). Note that the effective mass M^* as a function of B does not have a maximum. As y increases, the derivative $-dM_N(y)/dy$ has a maximum at the inflection point of the effective mass function $M^*(y)$, and then becomes a decreasing function of $y = T/B$, see the inset of Figure 1. When using the variable $y = T/B$, we come to the conclusion that as the temperature decreases, the leading edge of the function $-dS/dB = -dM^*/dT$ becomes steeper, and its maximum becomes higher [24]. These observations are in quantitative agreement with the striking measurements of the magnetization difference as a function of T/B obtained on both $Sr_3CuNb_2O_9$ [16] and $YbRh_2Si_2$ [23], as it is seen from Figure 4a,b. To perform a quantitative analysis of the scaling behavior of $-dM^*(B,T)/dT$, we calculate the entropy $S(B,T)$ as a function of B at fixed dimensionless temperatures T/μ shown in the upper right corner of Figure 4b [24]. Our theoretical curves in Figure 4a,b are shown in red [24]. In Figure 4a the NFL behavior and $\frac{dM}{dT}(T/B) \propto (T/B)^{-5/3}$ at $T/B > 1$ is shown by arrows. From Equations (9) and (10) it follows directly that in the NFL region the function $F(T/B) \propto -(5/3)$, as shown in Figure 4a. Our theoretical curves are displayed in Figure 4a,b. It is evident from Figure 4a,b that our calculations agree well with the experimental facts, and both scaled experimental dM/dT functions show scaling behavior over four decades in the variable T/B.
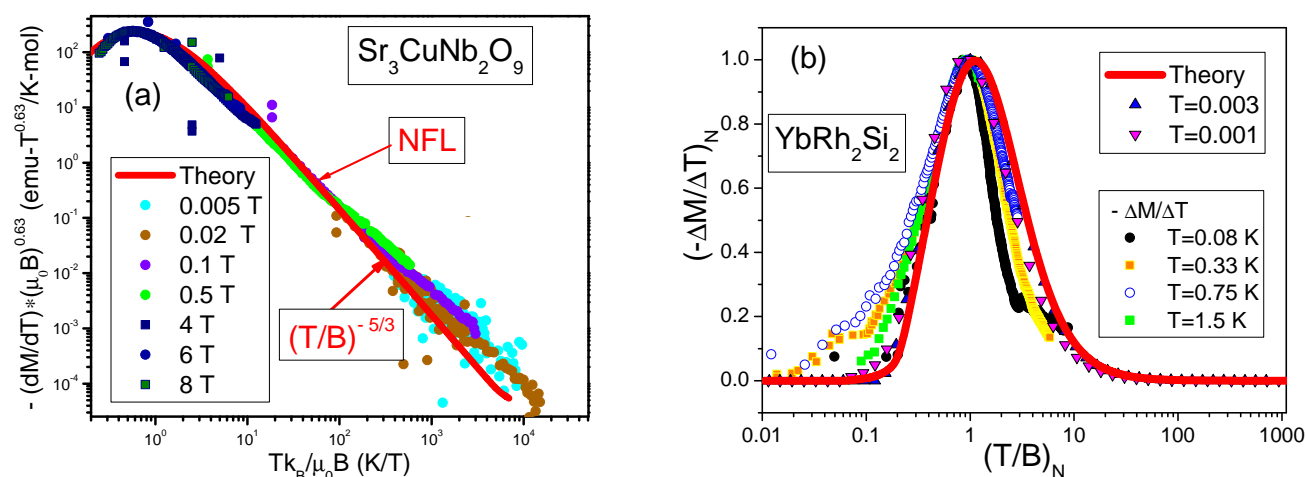

Figure 4. Scaled magnetization difference dM/dT versus scaled variable T/B. Panel (**a**): Scaling behavior of the magnetization $(dM/dT)\mu_0 B^{0.63}$ as a function of $Tk_B/\mu_0 B$ collected on $Sr_3CuNb_2O_9$ in a wide range of applied magnetic fields from 0.005 T to 8 T [16]. Our calculations are shown by the red curve that coincides with that shown in panel (**b**). At high temperatures $T/B > 1$ the system exhibits the NFL behavior with $\frac{dM}{dT}(T/B) \propto (T/B)^{-5/3}$. Panel (**b**): Normalized magnetization difference dM/dT collected on $YbRh_2Si_2$ versus scaled variable $(T/B)_N$ is extracted from the facts collected on $YbRh_2Si_2$ [23]. Our calculations of the normalized magnetization difference vs normalized T/B are given at fixed dimensionless temperatures T/μ (listed in the legend in the upper right corner). All data is represented by geometric figures shown in the legend in the upper left corner.

Figure 5a–c present the normalized specific heat capacity $(C_m/T)_N$ extracted from measurements of three different HF compounds. Two of them are represented by frustrated magnets: $Sr_3CuNb_2O_9$ [16] and $ZnCu_3(OH)_6Cl_2$ [25]. While the third one is the archetypical HF metal $YbRh_2Si_2$ [26,27]. According to the phase diagram shown in Figure 1, it is seen from Figure 5a–c that as temperature increases ($T/B_N \simeq 1$), the LFL behavior first transforms into a crossover and then breaks down into an NFL behavior. This demonstrates that the spin liquid of both $ZnCu_3(OH)_6Cl_2$ and $Sr_3CuNb_2O_9$ is close to the topological FCQPT and behaves as the HF liquid of $YbRh_2Si_2$. It is seen from Figure 5 that our calculations are in good agreement with the measurements. The agreement between the theory and the facts is good, and Equation (4) provides a good description of the scaling behavior of wide variety of HF compounds. As a result, we confidently conclude that the 3D quantum spin liquid is represented by SCQSL and $Sr_3CuNb_2O_9$ joins the family of the new state of matter [5].
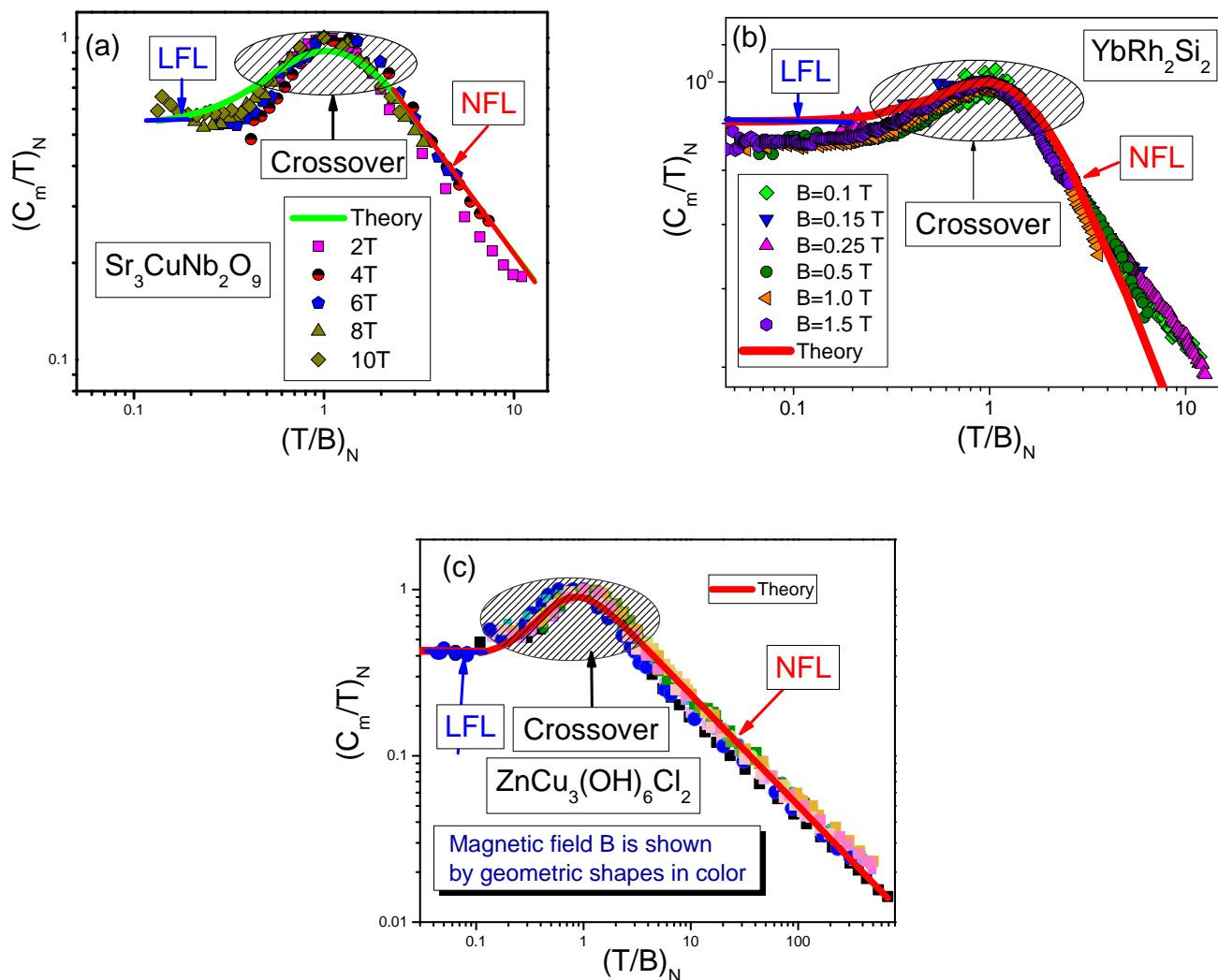
Figure 5. The normalized specific heat $(C_m/T)_N = M_N^*$ versus the normalized scaled variable $(T/B)_N$. Panel (**a**): $(C_m/T)_N$ is extracted from measurements on $Sr_3CuNb_2O_9$ under the application of magnetic field B shown in the legend [16]. Panel (**b**): $(C_m/T)_N$ is extracted from measurements on $YbRh_2Si_2$ under the application of magnetic field B shown in the legend [26,27]. Panel (**c**): $(C_m/T)_N$ is extracted from measurements on $ZnCu_3(OH)_6Cl_2$ measured under the application of magnetic field $0.1\,T \leq B \leq 14.0\,T$ [25]. For $Sr_3CuNb_2O_9$, $YbRh_2Si_2$ and $ZnCu_3(OH)_6Cl_2$ our calculations are represented by the same solid curve, see Equation (4). The curve traces the LFL behavior, the crossover and the NFL behavior.

4. Conclusions

Studies of flat bands are currently of great interest, see e.g., [2,6]. From an experimental point of view, one of their most important features is that when partially filled, they have an exponentially large number of states. This macroscopic degeneracy is due to the FC phenomenon generated by the topological FCQPT, which forms a self-consistent theory for all strongly correlated physics and explains the existence of a new state of matter that includes such insulating substances as geometrically frustrated magnets [1,5]. In our paper we have shown that the FC theory describes the facts of quantum frustrated magnets independently of their microscopic details or the combination of impurities and defects in each particular substance. We have shown that the scaling procedure makes it obvious that the experimental results on thermodynamic properties obtained on frustrated magnets and HF metals become identical. This shows the unity of the basic physics of these completely different solids that form a new state of matter. This unifying physical mechanism is driven by the FC phenomenon. Thus, we conclude that many unconventional objects that seem to be unrelated to each other, such as frustrated insulators, or magnets, and HF metals, can exhibit many similar but unexpected physical properties. Because these unrelated frustrated magnets have a common feature: flat bands arising from topological

FCQPT. It is the topological FCQPT that shapes the universal scaling behavior of strongly correlated Fermi systems; as a result, we boldly suggest that FC theory can provide a unified description of the properties of very different strongly correlated Fermi systems [1,5].

To summarize, the main goal of this paper is to reveal both the basic properties of QSL in quantum frustrated magnets and to draw attention to experiments that can clearly reveal the presence of SCQSL in frustrated insulators. Frustrated insulators are modern materials that have the properties of both insulators and metals, so they may find an outstanding place in future technologies. We have demonstrated that many seemingly unrelated experimental results can be well explained in terms of the hidden FC picture determined by the topological FCQPT generating flat bands, as we did for the disorder-induced 3D frustrated $Sr_3CuNb_2O_9$ magnet. We have shown that $Sr_3CuNb_2O_9$ can be viewed as a strongly correlated Fermi system whose thermodynamics is determined by the SCQSL located at the topological FCQPT. Our calculations of its thermodynamic properties agree well with experimental facts, and their scaling behavior is consistent with that observed in HF metals and other frustrated magnets. We also demonstrate that $Sr_3CuNb_2O_9$ exhibits LFL, NFL, and transient behavior similar to HF metals.

Acknowledgments

Author Contributions

V.R.S. and A.Z.M. designed the project and directed it with the help of S.A.A. and Y.S.L.; V.R.S. and A.Z.M. wrote the manuscript and all authors commented on it. The manuscript reflects the contributions of all authors. All authors have read and agreed to the published version of the manuscript.

Ethics Statement

Not applicable.

Informed Consent Statement

Not applicable.

Data Availibility Statement

The original contributions presented in the study are included in the article, further inquiries can be directed to the corresponding author.

Funding

Declaration of Competing Interest

The authors declare no conflicts of interest.

References

1. Shaginyan VR, Amusia MY, Msezane AZ, Popov KG. Scaling Behavior of Heavy Fermion Metals. *Phys. Rep.* **2010**, *492*, 31.

2. Heikkila TT, Volovik GE. Flat Bands as a Route to High-Temperature Superconductivity in Graphite. In *Basic Physics of Functionalized Graphite*; Esquinazi P, Eds.; Springer Series in Materials Science; Springer: Cham, Switzerland, 2016; Volume 244.

3. Checkelsky JG, Bernevig BA, Coleman P, Si Q, Paschen S. Flat bands, strange metals, and the Kondo effect. *Nat. Rev. Mater.* **2024**, *9*, 509.

4. Khodel VA, Shaginyan VR, Khodel VV. New approach in the microscopic Fermi systems theory. *Phys. Rep.* **1994**, *249*, 1.

5. Amusia MY, Shaginyan VR. *Strongly Correlated Fermi Systems: A New State of Matter*; Springer Tracts in Modern Physics Vol. 283; Springer Nature: Cham, Switzerland, 2020.

6. Regnault N, Xu Y, Li M-R, Ma D-S, Jovanovic M, Yazdani A, et al. Catalogue of flat-band stoichiometric materials. *Nature* **2022**, *603*, 824.

7. Khodel VA, Shaginyan VR. Superfluidity in system with fermion condensate. *JETP Lett.* **1990**, *51*, 553.

8. Peotta S, Törm P̈. Superfluidity in topologically nontrivial flat bands. *Nat. Comm.* **2015**, *6*, 8944.

9. Shaginyan VR, Stephanovich VA, Msezane AZ, Japaridze GS, Clark JW, Amusia MY, et al. Theoretical and experimental developments in quantum spin liquid in geometrically frustrated magnets: a review. *J. Mater. Sci.* **2020**, *55*, 2257.

10. Shaginyan VR, Msezane AZ, Japaridze GS, Artamonov SA, Leevik YS. Strongly Correlated Quantum Spin Liquids versus Heavy Fermion Metals: A Review. *Materials* **2022**, *15*, 3901.

11. Shaginyan VR, Msezane AZ, Japaridze GS. Peculiar Physics of Heavy-Fermion Metals: Theory versus Experiment. *Atoms* **2022**, *10*, 67.

12. Törmä P, Peotta S, Bernevig BA. Superfluidity and Quantum Geometry in Twisted Multilayer Systems. *Nat. Rev. Phys.* **2022**, *4*, 528.

13. Xu SY. Electronic transport goes quantum at room temperature. *Nat. Phys.* **2024**, *20*, 1047.

14. Shaginyan VR, Msezane AZ, Artamonov SA. General Properties of Conventional and High-Temperature Superconductors. *Crystals* **2024**, *14*, 826.

15. Bouzerar G, Thumin M. Hidden symmetry of Bogoliubov de Gennes quasi-particle eigenstates and universal relations in flat band superconducting bipartite lattices. *SciPost Phys. Core* **2024**, *7*, 018.

16. Hossain SM, Rahaman SS, Gujrati H, Bhoi D, Matsuo A, Kindo K, et al. Evidence of random spin-singlet state in the three-dimensional quantum spin liquid candidate $Sr_3CuNb_2O_9$. *Phys. Rev. B* **2024**, *110*, L020406.

17. Shaginyan VR, Msezane AZ, Popov KG. Thermodynamic properties of the kagome lattice in herbertsmithite. *Phys. Rev. B* **2011**, *84*, 060401(R).

18. Shaginyan VR. Density functional theory of fermion condensation. *Phys. Lett. A* **1998**, *249*, 237.

19. Landau LD. The Theory of a Fermi Liquid. Sov. Phys. *JETP* **1956**, *3*, 920.

20. Clark JW, Khodel VA, Zverev MV. Anomalous low-temperature behavior of strongly correlated Fermi systems. *Phys. Rev. B* **2005**, *71*, 012401.

21. Shaginyan VR, Popov KG, Stephanovich VA, Fomichev VI, Kirichenko EV. High-magnetic-fields thermodynamics of the heavy-fermion metal $YbRh_2Si_2$. *EPL* **2011**, *93*, 17008.

22. Helton JS, Matan K, Shores MP, Nytko EA, Bartlett BM, Qiu Y, et al. Dynamic Scaling in the Susceptibility of the Spin-1/2 Kagome Lattice Antiferromagnet. *Phys. Rev. Lett.* **2010**, *104*, 147201.

23. Tokiwa Y, Radu T, Geibel C, Steglich F, Gegenwart P. Divergence of the Magnetic Grüneisen Ratio at the Field-Induced Quantum Critical Point in $YbRh_2Si_2$. *Phys. Rev. Lett.* **2009**, *102*, 066401.

24. Shaginyan VR, Amusia MY, Popov KG. Strongly correlated Fermi-systems: non-Fermi liquid behavior, quasiparticle effective mass and their interplay. *Phys. Lett. A* **2009**, *373*, 2281.

25. Murayama H, Tominaga T, Asaba T, Silva AO, Sato Y, Suzuki H, et al. Universal scaling of specific heat in the $S = 1/2$ quantum kagome antiferromagnet herbertsmithite. *Phys. Rev. B* **2022**, *106*, 174406.

26. Gegenwart P, Tokiwa Y, Westerkamp T, Weickert F, Custers J, Ferstl J, et al. High-field phase diagram of the heavy-fermion metal $YbRh_2Si_2$. *New J. Phys.* **2006**, *8*, 171.

27. Oeschler N, Hartmann S, Pikul AP, Krellner C, Geibel C, Steglich F. Low-temperature specific heat of $YbRh_2Si_2$. *Physica B* **2008**, *403*, 1254.